Fermilab

Fermi National Accelerator Laboratory
P.O. Box 500 • Batavia, Illinois • 60510

TD-97-045
October 3, 1997

End Field Analysis for HGQ Model S02

G. Sabbi

Abstract:
In this note a magnetic field analysis for the end regions of the HGQ model S02 is presented.

1 Introduction

The first design iteration of the HGQ coil ends consisted of a magnetic analysis and optimization of the position of the conductor groups in the return end [1] followed by a detailed mechanical design of both the return and the lead end parts [2, 3]. This design has been adopted for the HGQS01 model. For the HGQS02 model, however, the second-wound conductor group in the outer coil is shifted outwards by 2 cm with respect to its original position. This decision has been taken after a new magnetic analysis of the baseline design [4] has shown that the peak field in the coil end is higher than previously indicated and that the short sample performance of HGQS01 is limited by the peak field in the return end. The modified geometry allows to reduce the peak field with only minor changes of the end parts. No significant degradation of the field quality is observed. In this note, an analysis of the magnetic field in the end regions of the HGQS02 model is presented. These calculations have been performed using the program ROXIE [5].

2 Computer model

The end design for model S02 follows the HGQ baseline geometry described in [2, 3], with the exception that the first wound conductor group of the outer coil is shifted by 2 cm in the positive z direction with respect to its original position. This transformation has been applied to both the return and the lead end. Figure 1 shows a longitudinal section of the return end at the pole angle for the modified geometry, and the corresponding geometry for the baseline design. The z-axis is directed outwards from the magnet body, and its origin is chosen following the definition in [2]. The iron yoke starts at at z=-5 cm for the return end, at z=-15 cm for the lead end.

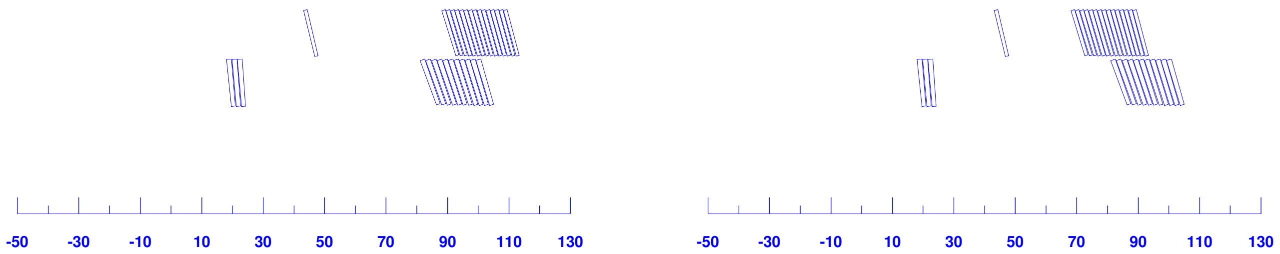

Figure 1: Longitudinal section at the pole angle for the return end of HGQ model #2 (left) as compared to the HGQ baseline design (right). Axis scale is in mm.

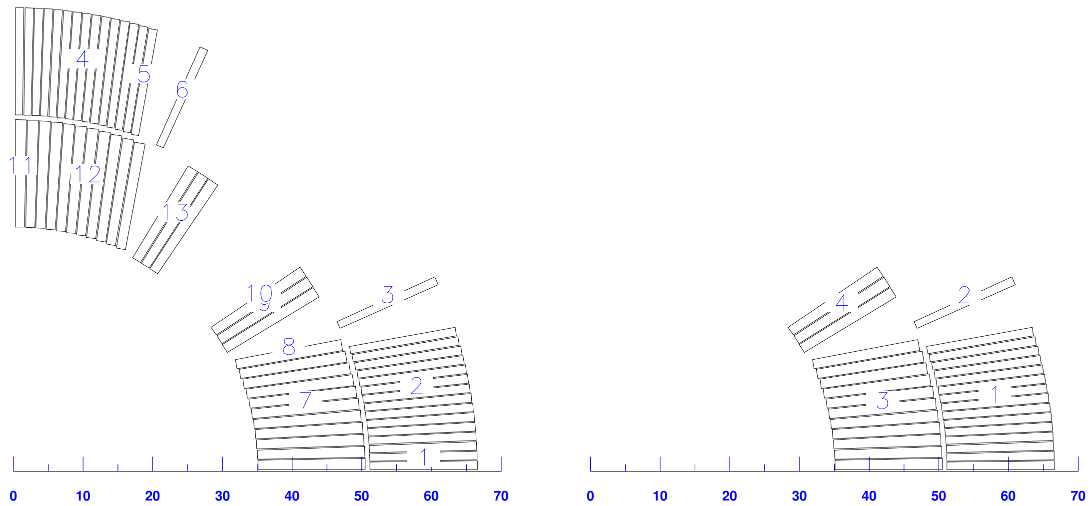

Figure 2: Coil cross-section model for the lead and return end. Axis scale is in mm.

The 3D model for the coil end regions is built by extrusion along the z axis, starting from a 2D model of the magnet cross-section. For the return end, which has exact quadrupole symmetry, it is sufficient to define the cross-section of one octant of the magnet, while for the lead end, where the coil is not symmetric with respect to the pole plane, it is necessary to define both the left and the rigth side of each quadrant (coil). The cross-section definitions for the blocks in the lead and return end are shown in figure 2 and tables 1 and 2. Both the blocks and the conductors are numbered from the mid-plane side to the pole side, starting with the outer layer.

ROXIE		BEND	No. turns	Description
Block #	Turn #	Group		
1	1 to 15	q2or312	15	2^{nd} wound, outer
2	16	q1or01	1	1^{st} wound, outer
3	17 to 27	q2ir29	11	2^{nd} wound, inner
4	28 to 30	q1ir03	3	1^{st} wound, inner

Table 1: Block and turn definitions for the HGQ return end. The same definitions apply in the magnet body.

ROXIE				BEND	No. turns	Description
Blk	Turn	Conn. blk	End type	Group		
1	1		1		1	Straight to quadrant splice
2	2 to 15	4	2	q2ol311	14	2^{nd} wound, outer, left
3	16	5	3	q1or01	1	1^{st} wound, outer, left
4	17 to 30	2	7	q2ol212	1	2^{st} wound, outer, right
5	31	3	8	q1ol01	1	2^{st} wound, outer, right
6	32	10	12	qoa/b	1	Ramp to coil spilce (outer)
7	33 to 42	12	4	q2il19	10	2^{nd} wound, inner, left
8	43	13	5	q1il01	1	2^{nd} wound, inner, left
9	44 to 45	13	6	q1il02	2	1^{st} wound, inner, left
10	46	6	13	qia/b	1	Ramp to coil splice (inner)
11	47		9		1	Straight to quadrant splice
12	48 to 57	7	10	q2il28	10	2^{nd} wound, inner, right
13	58 to 60	8,9	11	q1ir03	3	1^{st} wound, inner, right

Table 2: Block and turn definitions for the HGQ lead end.

The data for the 3D extrusion is obtained by reading into the ROXIE program the BEND coordinates files which specify the cross-sections of each conductor at small intervals along z. For the return end, 20 cross-sections have been specified from the edge of the iron yoke to the coil termination. The cross-sections are spaced more closely in those regions where the bending radius is smaller. For the lead end 3D extrusion, 30 cross-sections have been specified from the edge of the iron yoke to the coil termination. The coil to coil splice length is 11.43 cm. The quadrant splices are not included in the model; for each coil, the two connection conductors extend straight from the magnet body in the z direction and are truncated at z=15 cm.

Figure 3 shows the resulting ROXIE model for the lead and return end. The lead and return end calculations are performed separately. In each case, a straight section extending from the edge of the iron yoke for 1.5 m in the negative z direction is also included in the model.

The field calculation is based on the Biot-Savart law. The iron yoke is regarded as a magnetic mirror of circular shape (inner radius 9.256 cm) with infinite permeability. For the ROXIE calculation, each conductor has been subdivided in current filaments, one for each strand. The total number of strands is 38 in the inner layer, 46 in the outer layer. For both the lead and the return end calculations, a straight section extending in the negative z direction for 1.5 m from the start of the iron yoke towards the magnet body has been assumed.

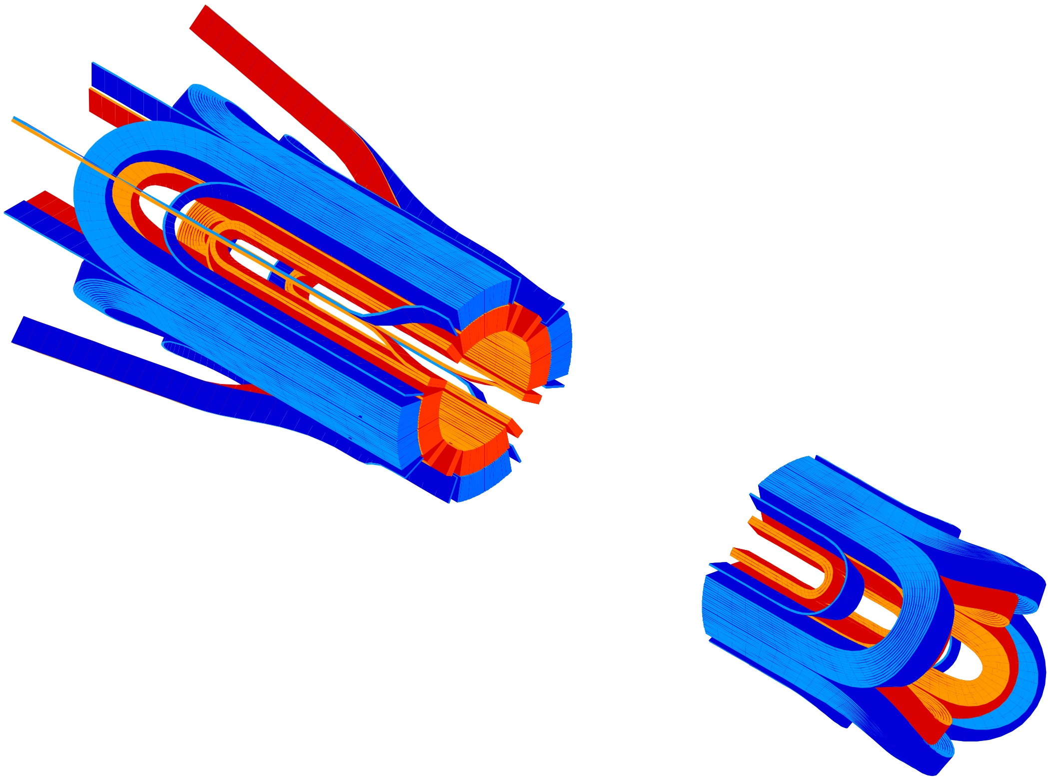

Figure 3: ROXIE model for the lead and return end of HGQS02.

2.1 Peak field

For the 3D peak field calculation, the method implemented in ROXIE does not allow to take into account the contribution of the iron yoke. This means that the field values calculated in the proximity of the edge of the iron yoke (z=-50 mm for the return end, z=-150 mm for the lead end) are incorrect. However, the actual peak field normally occurs close the coil edge, and previous calculations [1] show that in the case of HGQ the iron yoke is terminated at a sufficiently large distance from this region to ensure that its contribution to the peak field can be neglected.

Return end				Lead end			
Block	Turn	B^{max}/I (T/kA)		Block	Turn	B^{max}/I (T/kA)	
		HGQS02	HGQS01			HGQS02	HGQS01
1	15	0.573	0.599	1	1	0.419	0.419
2	16	0.536	0.541	2	15	0.571	0.576
3	27	0.635	0.599	5	31	0.554	0.556
4	30	0.654	0.656	6	32	0.401	0.401
				8	43	0.596	0.597
				10	46	0.639	0.639
				11	47	0.566	0.566
				12	56	0.609	0.588
				13	60	0.639	0.639

Table 3: Field load line coefficients in the HGQS02 lead and return end regions, and corresponding values for the HGQ baseline design [4].

Block	Turn	B^{max}/I (T/kA)	
#	#	I=1kA	I=14kA
1	15	0.596	0.576
2	16	0.588	0.567
3	27	0.649	0.631
4	30	0.707	0.687

Table 4: Field load line coefficients in the magnet body, at low and high current [6].

The linear coefficients for the maximum field in each block of the lead and return end as function of current are reported in table 3 for both HGQS02 and the baseline design. The corresponding coefficients calculated in the magnet body (taking into account the iron saturation and the detailed iron cross-section) are reported in table 4. As can be seen, the peak field in conductor 15 of the return end is decreased by about 4.5% with the new configuration, and is now slightly lower than the corresponding peak field in the straight section. To further increase the margin, more radical changes in the end configuration would be necessary. The peak field in the inner layer block 3 of the return end has increased, but remains lower than the corresponding maximum in block 4 and in the magnet body. In the lead end, where the second-wound groups of both the inner and the outer layer have one less conductor, the peak field is consistently lower than in the return end. No problem arises at the location of the splice ramps and current leads.

Figure 4 shows a comparison between the HGQ baseline design and the modified geometry of HGQS02 for what concerns the peak field in block 1 of the return end. As can be seen, the peak field enhancement at the pole has been eliminated.

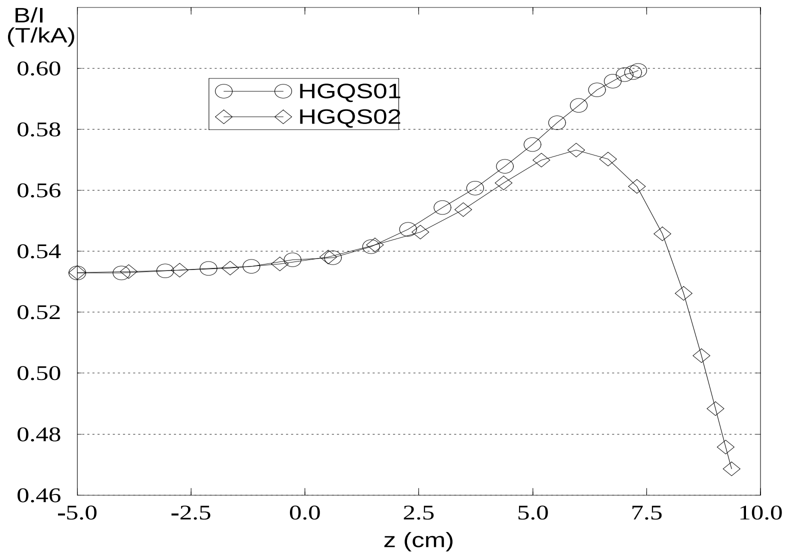

Figure 4: Comparison between field load line as function of z for conductor 15 in the return end of HGQS02 and corresponding plot for HGQS01 [4].

3 Field quality

The field quality in the end regions will be expressed in terms of integrated multipole components, defined according to the following expression:

$$\int_{z_p}^{z_q} [B_y(x,y,z) + iB_x(x,y,z)]dz = \sum_{n=1}^{\infty} (\hat{B}_n{}^{[z_p,z_q]} + i\hat{A}_n{}^{[z_p,z_q]}) \left(\frac{x+iy}{r_0}\right)^{n-1} \tag{1}$$

This expansion is only valid if the integration interval covers the whole end region, i.e. if the starting point z_p is sufficiently inside the magnet body and the end point z_q is sufficiently far away from the coil termination. In general, the expansion for the 3D field in the end regions would require additional terms (pseudo-multipoles). However, the pseudo-multipole components integrate to zero and can therefore be eliminated provided that the longitudinal field component vanishes at the boundaries of the integration interval [7].

As for the magnet straigth section, it is convenient to express the integrated multipole components $\hat{B}_n$, $\hat{A}_n$ in the end regions in "units" of 10^{-4} of the main integrated quadrupole field $\hat{B}_2^{[z_p,z_q]}$:

$$\hat{b}_n^{[z_p,z_q]} = \frac{\hat{B}_n^{[z_p,z_q]}}{\hat{B}_2^{[z_p,z_q]}} \cdot 10^4 \tag{2}$$

$$\hat{a}_n^{[z_p,z_q]} = \frac{\hat{A}_n^{[z_p,z_q]}}{\hat{B}_2^{[z_p,z_q]}} \cdot 10^4 \tag{3}$$

The magnetic length L_m of the interval $[z_p, z_q]$ is defined as the length of straigth section which would provide an equivalent integrated strength for the main (quadrupole) field component:

$$L_m^{[z_p,z_q]} = \frac{\hat{B}_2^{[z_p,z_q]}}{B_2} \tag{4}$$

For the present study, the integrated multipoles have been obtained from 50 line integrals of the transverse field, calculated along lines parallel to the z-axis, at the reference radius of 1 cm and equally spaced azimuthal angles. The integration limits are [-25,+25] cm for the return end and [-35,+25] cm for the lead end. This ensures that the longitudinal component of the magnetic field at the boundaries of the integration intervals is negligibly small and that the field integral can be expanded according to equation 1. Each field integral has been evaluated by adding up the contributions calculated at 1 mm intervals along z. The magnetic length calculation is based on a transfer function in the magnet body of 18.22 T/m/kA, as obtained for a 2D analysis carried out under the same assumptions (conductors aligned to the coil outer radius, circular iron yoke of inner radius 9.2564 cm and infinite permeability) [6]. The results for the magnetic length and the average multipole components in the HGQ lead and return end regions are reported in table 5 and 6. As can be expected, a slight increase in magnetic length is observed with the new configuration. For what concerns the field quality, the $\hat{b}_6$ component is slightly higher in both the return and the lead end, while a reduction of the skew terms $\hat{a}_2$ and $\hat{a}_6$ in the lead end is observed. The change in the higher order terms (n=10, 14) of both the return and the lead end is negligible.

In order to carry out a beam tracking analysis where the local variation of the field is taken into account, a 3D expansion for the local (longitudinal and transverse) field in terms of pseudo-multipoles is needed. This expansion can be built starting from the field values $\vec{B}(r_0, \theta_i, z_j)$ calculated on a cylindrical surface inside the magnet bore [8]. These data have been calculated for $r_0 = 1$ cm, at 50 different angles and 1 mm longitudinal spacing, and are available upon request.

Parameter	HGQS02	HGQS01
L_m (cm)	41.39	40.72
$\hat{b}_2$	10000	10000
$\hat{b}_6$	0.657	0.597
$\hat{b}_{10}$	-0.0032	-0.0032
$\hat{b}_{14}$	-0.000015	-0.000015
$\hat{a}_2$	38.54	42.8
$\hat{a}_6$	0.020	0.025
$\hat{a}_{10}$	-0.0011	-0.0011
$\hat{a}_{14}$	0.000007	0.000006

Table 5: Integrated harmonic coefficients for the lead end of HGQS02, as compared to the HGQ baseline end design [4]. The integration interval starts at z=-35 cm and ends at z=+25 cm.

Parameter	HGQS02	HGQS01
L_m (cm)	32.50	31.78
$\hat{b}_2$	10000	10000
$\hat{b}_6$	0.140	0.048
$\hat{b}_{10}$	-0.0040	-0.0041
$\hat{b}_{14}$	-0.000017	-0.000017

Table 6: Integrated harmonic coefficients for the return end of HGQS02, and corresponding values for the HGQ baseline end design [4]. The integration interval starts at $z = -25$ cm and ends at z=+25 cm.

4 Conclusions

The modified configuration of the second-wound conductor group of the lead and return ends of HGQS02 allows to decrease the peak field and to improve the magnet short sample performance up to the limit calculated for the magnet body. From the field quality standpoint, the new configuration is substantially equivalent to the HGQ baseline design.

References

[1] S. Caspi, *"LHC IR Quad"*, FNAL/LBL/CERN videoconference meeting, May 1st, 1996.

[2] J. Brandt, A, Simmons, *"Coil End Design for the LHC IR Quadrupole Magnet"*, Fermilab TS-96-013, November 1996.

[3] J. Brandt, *"Preform and Pole Splice Design for the LHC IR Quadrupole Magnet"*, Fermilab TS-96-014, November 1996.

[4] G. Sabbi, *"Magnetic Field Analysis of HGQ Coil Ends"*, Fermilab TD-97-040, September 1997.

[5] S. Russenschuck, *"A computer program for the design of superconducting accelerator magnets"*, Proc. ACES Symposium, Monterey, California, 1995 and CERN AT/95-39, September 1995.

[6] G. Sabbi, *"Load lines and short sample limits for HGQ model S01"*, Fermilab TD-97-011, April 1997.

[7] S. Caspi, M. Help, L. Laslett, *"3D Field Harmonics"*, LBL Report SC-MAG-328, March 1991.

[8] S. Caspi, M. Helm, L. Laslett, V. Brady, *"An approach to 3D Magnetic Field Calculation Using Numerical and Differential Algebra Methods"* LBL SC-MAG-395, July 1992.